Zeng et al. Journal of Palaeogeography (2019) 8:18
https://doi.org/10.1186/s42501-019-0033-7

Journal of Palaeogeography

ORIGINAL ARTICLE Open Access

Palaeoenvironmental setting of lacustrine stromatolites in the Miocene Wudaoliang Group, northern Tibetan Plateau

Ling-Qi Zeng[1], Hai-Sheng Yi[1,2*], Guo-Qing Xia[1,2], Klaus Simon[3], Christine Heim[3] and Gernot Arp[3]

Abstract

Lacustrine stromatolites were widespread in the Miocene Wudaoliang Group (stromatolites of the Wudaoliang Group), northern Tibetan Plateau; but only at one location nearby the Wudaoliang Town, they occurred intensively in thick, laterally traceable beds (Wudaoliang stromatolites). Although deposited in lacustrine environment, the lack of fossils in these rocks hampers determining whether the stromatolites formed in freshwater or saline conditions. To address this problem, and in an attempt to identify criteria to distinguish differences of freshwater and saline conditions, we studied the laminae microfabrics, stable carbon and oxygen isotope ratios, rare earth element patterns and biomarkers of the stromatolites. These stromatolites can be divided into fenestral stromatolites and agglutinated stromatolites. The fabric of fenestral stromatolites is formed by microcrystalline carbonate enclosing spar-cemented, angular crystal traces. Essentially, this fabric is interpreted as pseudomorph after former formed evaporite crystals. Faecal pellets identical to that of the present-day brine shrimp *Artemia*, lack of other eukaryotic fossils, and stable isotopic signals point to a shallow, evaporation-dominated hypersaline lake setting. Covariation of carbon and oxygen isotopes indicates hydrologically closed conditions of the Miocene lake on northern Tibetan Plateau.

However, if compared to other lacustrine carbonates of the Wudaoliang Group, the high $\delta^{13}C$ values of the investigated Wudaoliang stromatolites reveal an additional photosynthetic effect during the deposition of the stromatolites. Furthermore, although no direct evidence is available from field observations and microfabrics, a positive europium anomaly of Wudaoliang stromatolites indicates that a palaeo-hydrothermal inflow system had existed in the outcrop area. These new results favour a hypersaline lake setting subject to hot spring inflow for the Wudaoliang stromatolites, in contrast to earlier interpretations suggesting a freshwater lake setting (e.g. Yi et al., Journal of Mineralogy and Petrology 28: 106–113, 2008; Zeng et al., Journal of Mineralogy and Petrology 31: 111–119, 2011). This approach may be appropriate for other lacustrine, unfossiliferous microbialites in settings where the environmental conditions are difficult to determine.

Keywords: Lacustrine stromatolites, Miocene Wudaoliang Group, Hypersaline lake, Hydrothermal, Northern Tibetan plateau

1 Introduction

Microfabrics and geochemical features of lacustrine stromatolites are valuable indicators of palaeoenvironmental changes in continental settings otherwise rare in fossils (Monty 1976; Surdam and Wray 1976; Riding 2000). In this study, the environmental conditions of extensive lacustrine stromatolites are investigated using a combination of petrography and geochemistry to resolve existing issues about controls on their formation. Lacustrine stromatolites are common in the Miocene Wudaoliang Group in the northern Tibetan Plateau region (Qinghai Province), western China, and they usually occur as centimeter- to decimeter-thick beds intercalated between carbonates. But nearby Wudaoliang Town in particular, the stromatolites (also from the Wudaoliang Group) occur in an area of about $240 \times 80\ m^2$ in size, forming a total 15-m-thick bed, exposed on a hill slope (Fig. 1). We refer the former, centimeter- to decimeter-thick beds as stromatolites in the Wudaoliang Group and the latter nearby Wudaoliang Town, specifically, as Wudaoliang stromatolites. Yi et al. (2008) and

* Correspondence: yhs@cdut.edu.cn
[1]Institute of Sedimentary Geology, Chengdu University of Technology, Chengdu 610059, Sichuan Province, China
[2]State Key Laboratory of Oil and Gas Reservoir Geology and Exploitation, Chengdu 610059, Sichuan Province, China
Full list of author information is available at the end of the article

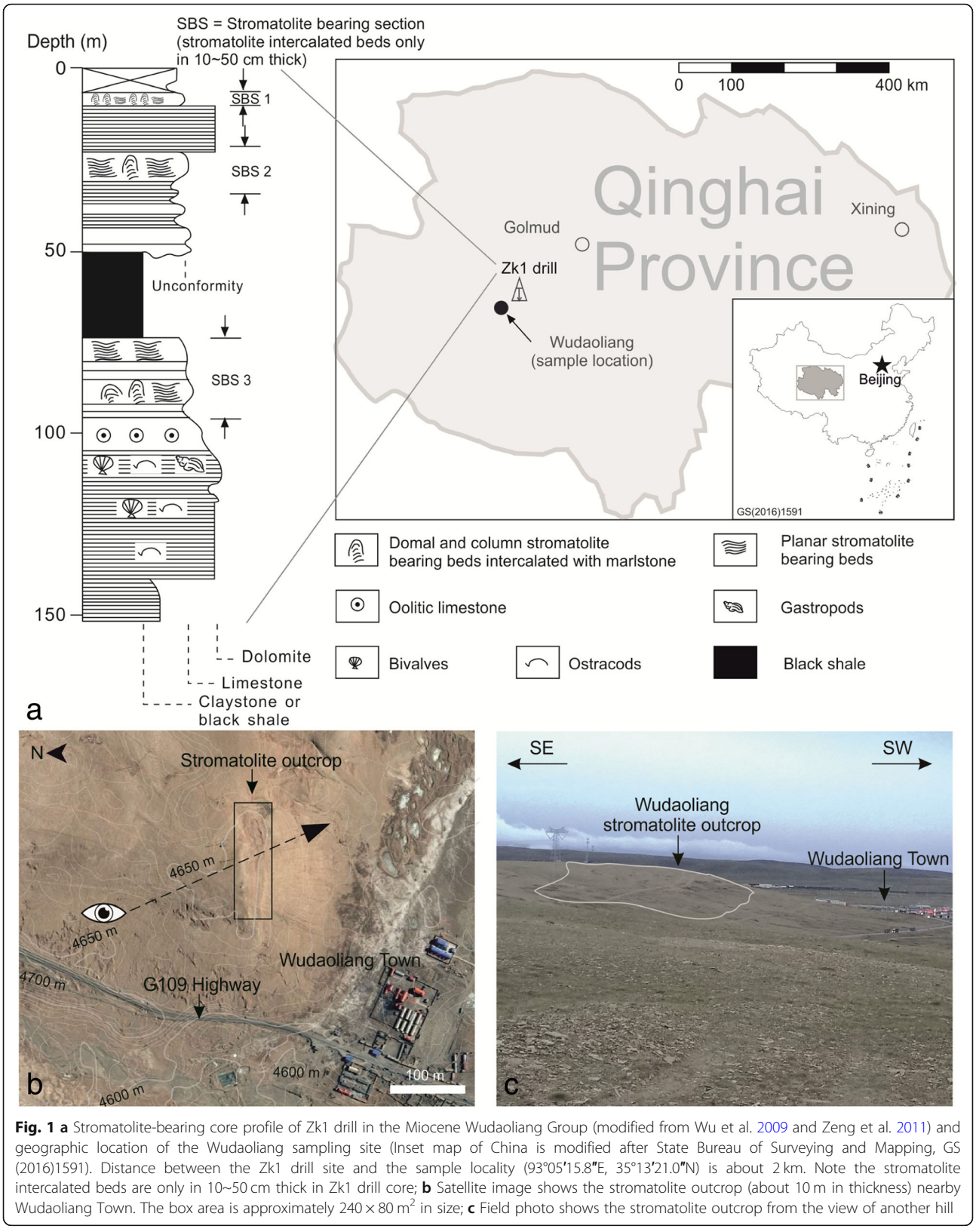

Fig. 1 **a** Stromatolite-bearing core profile of Zk1 drill in the Miocene Wudaoliang Group (modified from Wu et al. 2009 and Zeng et al. 2011) and geographic location of the Wudaoliang sampling site (Inset map of China is modified after State Bureau of Surveying and Mapping, GS (2016)1591). Distance between the Zk1 drill site and the sample locality (93°05′15.8″E, 35°13′21.0″N) is about 2 km. Note the stromatolite intercalated beds are only in 10~50 cm thick in Zk1 drill core; **b** Satellite image shows the stromatolite outcrop (about 10 m in thickness) nearby Wudaoliang Town. The box area is approximately 240 × 80 m^2 in size; **c** Field photo shows the stromatolite outcrop from the view of another hill

Zeng et al. (2011) inferred from stable isotopes that the stromatolites in the Wudaoliang Group formed in a freshwater lake and they interpreted a humid interval of the long-term, warm and dry Miocene palaeoclimate in northern Tibetan Plateau. However, typical skeletal fossils are very rare in stromatolites in the Wudaoliang Group, in contrast to the common occurrence of calcified cyanobacteria (Riding 1991), gastropods and ostracods (e.g., the Eocene Green River Formation, Surdam and Wray 1976) in freshwater lakes or rivers. Wudaoliang stromatolites possess substantial elongated, filament-like microcrystalline structures, with angular spar-cemented voids in between, reminiscent of former evaporite crystals. Similar crystal traces are known from other calcareous stromatolites of hypersaline settings (e.g., Arp et al. 2008). Furthermore, syn-sedimentary Pb-Zn deposits in the adjacent Tuotuohe Basin (Hao et al. 2015) suggest a possible hydrothermal impact also in the Wudaoliang Basin at that time (Zhang et al. 2015).

Thus, it is unknown whether these stromatolites formed in a freshwater setting, saline halite lake or soda lake conditions. Meanwhile, a possible hydrothermal impact on these stromatolites remains to be confirmed. In order to solve the undetermined issues of environmental conditions, this study examined the macrofabrics and microfabrics of the stromatolites, distinguished different laminae by the fabrics and geochemical composition, and discussed the genesis of the stromatolites. LA-ICP-MS was used to obtain high-resolution elemental data to analyse the potentially preferential elemental enrichment in different laminae and fabrics. Combined these results with stable oxygen and carbon isotopes, consequently, this study identified one kind of hypersaline lake environment during the Miocene stromatolites formation period, nearby the present Wudaoliang Town of Qinghai Province, northern Tibetan Plateau.

2 Geological settings

The investigated stromatolites belong to the carbonate-dominated Miocene Wudaoliang Group (marls, dolomites and limestones; 23.5–13.5 Ma) that unconformably overlies the Oligocene conglomerates and sandstones (Yaxicuo and Fenghuoshan Groups) in Wudaoliang and adjacent basins (Wu et al. 2008) in Hoh Xil area. Wudaoliang Group, Yaxicuo Group and Fenghuoshan Group were deposited in a lacustrine environment that developed in the northern Tibetan Plateau during its uplift, crustal shortening, and a general three-phase evolution of warm (dry)-cool (wet)-cool (dry) climate during the Oligocene-Miocene (Wu et al. 2008; Wang et al. 2008). The interconnected early-Miocene lake-basins were successively separated during their later evolution.

The 310–350-m-thick Wudaoliang Group shows only minor tectonic deformation, with inclined beds of tipping angle less than 30°, suggesting a comparatively weak tectonic-active episode in the Cenozoic of the northern Tibetan Plateau (Wang et al. 2002, 2008). The lower part of the Wudaoliang Group hosted marls with a wide spectrum of fresh- to brackish-water organisms (ostracods, gastropods), while its upper part was dominated by dolomites and limestones with intercalated stromatolites (Wu et al. 2008; Zeng et al. 2011).

The sampling site was located nearby Wudaoliang Town along the Qinghai-Tibet Highway (G109), 270 km south from the Golmud (GPS: 93°05′15.8″E, 35°13′21.0″N, H 4667 m; Fig. 1).

3 Material and methods

Three large thin-sections (all with a thickness of 80 μm, and two with a size of $10 \times 15\ cm^2$ and another of $4.5 \times 1.5\ cm^2$) and twenty standard thin-sections (30 μm thick) were used for petrographic investigation on a Zeiss Axioplan microscope (Carl Zeiss MicroImaging GmbH, Jena, Germany). Micro features were carefully studied under the microscope, to develop a clear understanding of the sedimentary fabric, before geochemical approaches were used.

3.1 Stable oxygen and carbon isotope analysis

One fresh stromatolite cut slab was drilled to obtain microcrystalline calcite samples from each individual lamina. In each lamina at least two microcrystalline calcite samples were drilled. Totally, 89 calcite samples were obtained in 36 continuous, alternating dense and porous laminae towards one linear direction within one stromatolite cut slab. The 89 powdered calcite samples were then prepared and analysed by a Finnigan MAT 252 mass spectrometer. Both carbon and oxygen isotopes of the stromatolitic limestone were analyzed under the Vienna Peedee Belemnite standard (VPDB) and the results were given in δ‰.

3.2 LA-ICP-MS analysis

A 193 nm ArF excimer laser ablation system (LA, GeoLas, COMPEX 110, Lambda Physix, Germany) coupled to an Elan DRCII 6100 inductively coupled plasma-mass spectrometer (ICP-MS, PerkinElmer, Germany) was used for rare earth elemental measurements. The laser ablation was operated at a wavelength of 193 nm, energy density of $10\ J{\cdot}cm^{-2}$ and frequency of 10 Hz. Ablation spot size was set to 50 μm, and one fenestral stromatolite sample was analysed by the ablation spot mode: 120 calcite samples in 17 laminae were ablated (no less than 5 samples in each laminae). Furthermore, four 20-mm-long line-scan measurements vertically crossed laminae, were operated in two stromatolite slabs.

3.3 Carbon analysis

Organic and carbonate carbon contents were determined using LECO RC612 multiphase-carbon analyser. Organic carbon (C_{org}) was measured after decarbonization with 2 N HCl. Carbonate carbon (C_{carb}) was calculated as the difference of directly determined total carbon (C_{tot}) and organic carbon (C_{org}).

3.4 Biomarker analysis

Biomarkers were extracted using one freshly-cut stromatolite rock sample, and the surface layer was separately removed to avoid potential diagenetic alteration and contamination. Powders were extracted stepwise with distilled dichloromethane/methanol (3:1), dichloromethane (DCM), and *n*-hexane, using ultrasonication. After drying and derivatizing the extracted calcite powder was dissolved. The residue samples were centrifuged and neutralized by flushing with distilled water. Further biomarker extraction was also performed by ultrasonication with DCM/methanol (3:1), DCM and *n*-hexane. The total organic extract, lipid fraction and combined organic extract were analysed with Thermo

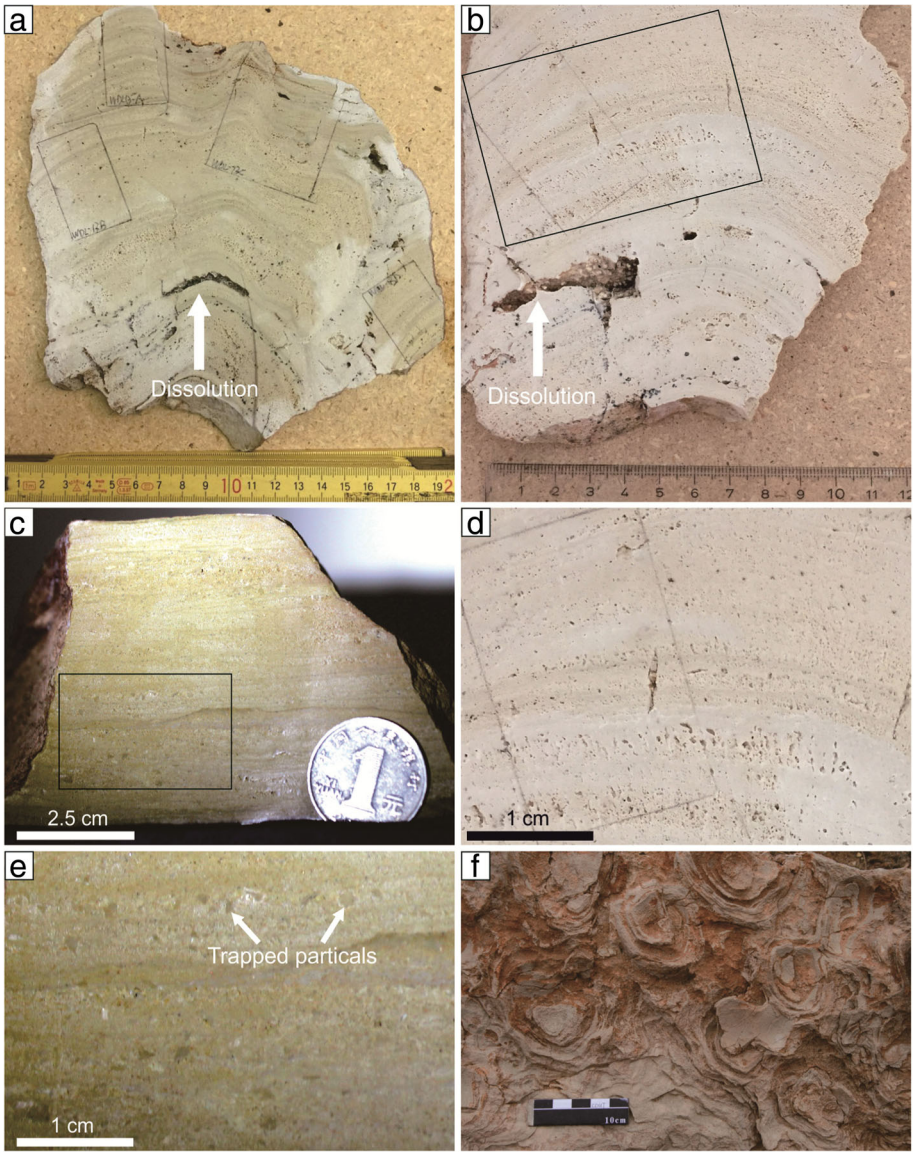

Fig. 2 **a** Vertically-cut slab of a representative fenestral stromatolite hand specimen (WDL-13). Large open voids result from late meteoric dissolution; **b** Vertically-cut slab of another fenestral stromatolite hand specimen (WDL-12); **c** Slab of agglutinated stromatolite with substantial trapped particles. Diameter of the coin is 2.5 cm; **d** Zoomed area of the fenestral stromatolite in Fig. 2b. Note the millimeter-scale, elongated voids vertically arrayed to the laminae; **e** Zoomed area (2.4× magnification) of the agglutinated stromatolite in Fig. 2c, showing trapped/bound particles in different size; **f** Field image of stromatolites of the Wudaoliang Group

Trace 1310 GC coupled to Thermo TSQ Quantum Ultra triple quadrupole MS.

4 Results

4.1 Classification, texture and fabrics of Wudaoliang stromatolites

Microscopic observations revealed that two different types of stromatolites developed in the investigated outcrop: the fenestral stromatolites and the agglutinated stromatolites.

4.1.1 Fenestral stromatolite

Fenestral stromatolite is characterized by spar-cemented voids (Fig. 2a and b). Following Demicco and Hardie (1994), fenestral fabrics are referred to millimetre-scale, open or spar-cemented voids formed during syn-depositional and early diagenetic phase. Two types of fenestrae, angular fenestrae and irregular fenestrae, can be recognized. Angular fenestrae (Fig. 3a and b) are essentially elongated structures enclosed by ~ 0.5–1.0 mm long micritic sublinear structures with sharp edges. Irregular fenestrae occur as millimeter-scale, open or spar-cemented cavities without defined shape (Figs. 2b, d, 3a-b).

Laminae types of fenestral stromatolites were subdivided by the type and abundance of fenestrae into three groups (Table 1): 1) spongy layers formed by upright oriented microcrystalline sublinear micrite structures enclosing elongated fenestrae (Fig. 3a and b); 2) clotted

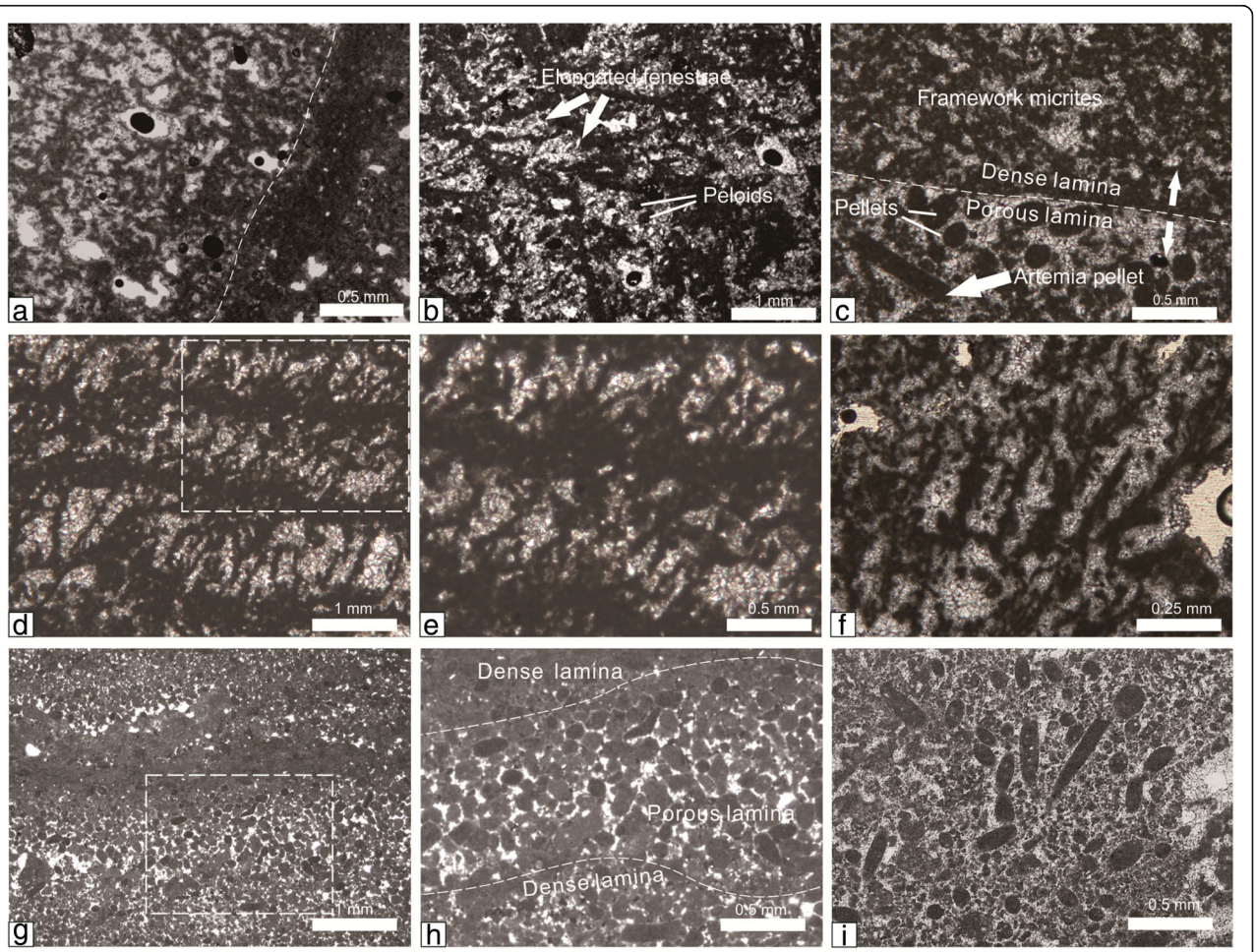

Fig. 3 Microscopic images of Wudaoliang stromatolites. **a** Porous lamina (left side of the dashed line) and clotted lamina (right side of the dashed line) of fenestral stromatolite; **b** Elongated fenestrae (arrows) in a spongy layer, with few peloids (lines) and detrital components; **c** Dense peloidal lamina (the upper) and porous peloidal lamina, and the arrow showed an elongated pellet resembled to *Artemia* pellet by similar size (380 μm long); **d** Microscopic image of the thin section of Fig. 2e, showing spongy layers (with voids and spar cements) alternated with thin microcrystalline layers (no voids or spar cements), and abundant fenestral fabrics in spongy layers; **e** Zoomed area of rectangle zone in the Fig. 3d. Note that the angular, microspar-filled crystals (or voids) are possibly traces of the former evaporite minerals; **f** Zoomed area of rectangle zone in the Fig. 3d; **g** Pellets-rich laminae of agglutinated stromatolites, either densely packed or loosely packed; **h** Zoomed area of rectangle zone in the Fig. 3g. Note the almost constant size of the pellets (refer to the Fig. 3i); **i** Different sized (up to 500 μm) faecal pellets due to cross-section (cutting) effect in an agglutinated stromatolite

Table 1 Classification of Wudaoliang stromatolites and laminae within

Stromatolite classification	Laminae type	Approximate thickness (mm) of laminae	Description
Fenestral stromatolite (Figs. 2a, b, d, 3a, b, d-f)	Porous (spongy) laminae	0.5–1.5	Fenestrae fabric components are > 25%. Angular and elongated fenestrae are filled with microspars, between the massive microcrystalline and the filament-like (0.1–0.2 mm in length and 20–50 μm in width) vertically structured micrites. The angular fenestrae are sub-rhombic calcite pseudomorphs after evaporite crystals, possibly gypsum.
	Clotted microcrystalline laminae	1–4	5%–25% fenestral (only tiny, irregular) fabric constitutes this kind of laminae. Irregular peloids of indistinct boundaries are closely clotted.
	Thin massive microcrystalline (aphanitic) laminae	0.15–0.20	Few or no fenestral fabric components. Smooth, slightly undulating massive microcrystalline calcite is the primary component for this kind of laminae; and no void structures are found in the thin section.
Agglutinated stromatolite (Figs. 2c, e, 3c-i)	Porous peloidal laminae (Fig. 3c, g)	1.0–1.2	No fenestrae and composed of trapping (binding) particles, i.e., peloidal micrites and faecal pellets. Particles are loosely piled or packed between the microspar cements. The size of pellets ranges from 20 μm to 500 μm.
	Dense peloidal laminae (Fig. 3c, g)	0.70–0.85	Primary components: densely packed pellets and peloids, microcrystalline dense calcite in fairly low porosity.

microcrystalline laminae containing irregular fenestrae; 3) dense microcrystalline (aphanitic) layers.

4.1.2 Agglutinated stromatolite

The investigated agglutinated stromatolite showed only minor fenestral fabrics (Fig. 2c). Instead, significant amounts of trapped and bound particles were observed (Figs. 2e, 3d-f). The particles could be divided into peloids, faecal pellets and framework micrites.

Peloids were microcrystalline grains without specific shape. Spherical, slightly elongated or even subangular peloids, sized from less than 10 μm to 100 μm. Peloids were generally surrounded by microspar cements, or irregularly clotted to other peloidal micrites.

Faecal pellets were composed of dark microcrystalline calcite and range in size from 80 μm to 120 μm (Fig. 3c, g, h). The length of some elongated pellets could attain 500 μm (Fig. 3i). The pellets showed no internal structures, and round to sub-round or elliptical shapes, occasionally broken into segments. Pellets were either bound and floated with the presence of other particles, or exclusively packed and stacked to form dense peloidal layers.

Framework micrite comprised micrite aggregates (sometimes including peloids and pellets) closely clotted to each other, causing the original periphery of particles to be no longer recognizable. Micrite was aggregated to form different morphological connections, which could be microscopically clotted, dendroid or thrombolitic-like aggregates.

Occurrences of irregular branching endolithic filaments, which were about 10 μm in diameter and locally penetrated the stromatolites on their surface layers, were confirmed as contaminations instead of primary fossils.

4.2 Stable carbon and oxygen isotope

Stable carbon and oxygen isotope results of Wudaoliang stromatolites are listed in Table 2 and plotted on Fig. 4. The $\delta^{13}C$ values of the analysed fenestral stromatolite ranged from 2.340‰ to 4.265‰, with a mean value of 3.030‰. The $\delta^{18}O$ values ranged from − 9.070‰ to − 6.095‰, with a mean value of − 7.394‰. Both carbon and oxygen isotopes showed slight oscillations in continuous alternating porous and dense laminae, with a mean $\delta^{13}C$ value of 0.289‰ and a mean $\delta^{18}O$ value of 0.514‰ in two adjacent laminae. However, there was no significant difference between porous (spongy) and dense (clotted) laminae. A positive covariation was evident between $\delta^{13}C$ and $\delta^{18}O$ ratios ($r = 0.720$, $n = 36$, $p < 0.05$).

4.3 Rare earth element (REE) pattern

The ablation spot measurements of laser ablation inductive coupled plasma-mass spectrometer were heterogeneous, possibly due to the low REE concentrations in carbonate minerals. To deduce this effect, we calculated the mean REE value of ablation spots in each lamina (Fig. 5). The very similar shale normalized REE patterns of laminae indicated that the heterogeneous signals could be eliminated by overlapping signals of the individual points. Similar integrations were made on the line-scan mode data.

The results of stromatolite samples analysed by LA-ICP-MS were shown in Tables 3, 4, 5 and 6. The ΣREE of the stromatolites ranged from 3392 ppb to 5746 ppb (Table 3). Nine dense laminae of the sample WDL-13-A had a mean ΣREE concentration of 6286 ppb, whereas the eight porous laminae in this sample yielded a mean ΣREE concentration of 4479 ppb (Table 5). REE data of Wudaoliang stromatolites and reference samples in Table 3 were also presented in Fig. 5, normalized by the Post-Archean Australian Shale (PAAS).

Table 2 Stable carbon and oxygen isotope results of Wudaoliang stromatolites

Lamina number	Lamina type	$\delta^{13}C$ (‰)	$\delta^{18}O$ (‰)
1	Porous	3.073	−7.810
2	Dense	3.170	−7.425
3	Porous	3.048	−7.318
4	Dense	3.080	−7.775
5	Porous	3.163	−6.817
6	Dense	2.755	−8.245
7	Porous	3.153	−6.625
8	Dense	3.160	−7.130
9	Porous	3.312	−7.288
10	Dense	3.170	−7.115
11	Porous	3.178	−7.175
12	Dense	3.615	−6.740
13	Porous	2.973	−7.323
14	Dense	2.930	−7.260
15	Porous	3.195	−7.235
16	Dense	2.835	−7.305
17	Porous	2.935	−7.350
18	Dense	2.730	−7.600
19	Porous	3.030	−7.775
20	Dense	3.055	−7.485
21	Porous	2.340	−9.070
22	Dense	4.265	−6.095
23	Porous	2.965	−7.715
24	Dense	2.955	−7.550
25	Porous	2.990	−7.655
26	Dense	2.820	−7.320
27	Porous	3.165	−7.305
28	Dense	2.990	−7.380
29	Porous	3.365	−7.130
30	Dense	2.880	−7.080
31	Porous	2.795	−8.268
32	Dense	2.850	−7.610
33	Porous	3.025	−7.240
34	Dense	2.775	−7.310
35	Porous	2.745	−7.575
36	Dense	2.600	−7.100
Max	Porous	3.365	−6.625
Min	Porous	2.340	−9.070
Avg	Porous	3.025	−7.482
Max	Dense	4.265	−6.095
Min	Dense	2.600	−8.245
Avg	Dense	3.035	−7.307
Max	All laminae	4.265	−6.095
Min	All laminae	2.340	−9.070
Avg	All laminae	3.030	−7.394
Standard diviation	All laminae	0.313	0.498
r-value	0.720	*p*-value	0.0000008

Except for WDL-13-D-1, the stromatolite samples showed positive Eu anomalies (Eu/Eu^*_{SN}) from 1.006 to 1.260 (Table 4). And, 14 of the 17 laminae in sample WDL-13-A showed positive Eu anomalies with a highest value of 1.608 (Table 6). In samples WDL-10-C-1, WDL-10-C-2 and WDL-13-A, La/Lu_{SN} ratios ranged from 0.568 to 0.794; and, La/Lu_{SN} ratios ranged from 0.944 to 0.955 in samples WDL-13-D-1 and WDL-13-D-2 (Table 4). Sample WDL-13-D-1 had a positive Ce anomaly of 1.300 (Table 4). However, 2 laminae in sample WDL-13-A showed negative Ce anomalies (0.360 and 0.627; Table 6).

4.4 Carbon content and biomarker analysis

The six analysed stromatolite samples had a carbonate content ranging from 94.9 wt% to 97.0 wt%, but the organic carbon content hardly reached 0.1 wt%.

The biomarker content of the analysed stromatolites was very low and mainly as hydrocarbon biomarkers, namely normal alkanes (n-alkanes) (Fig. 6). Branched or cyclic hydrocarbons were not observed. The distribution of hydrocarbon biomarkers ranged from C_{19} to C_{33} n-alkanes (C_{19} to C_{33}) with a bimodal pattern at C_{22} and C_{29} respectively (Fig. 6). The relative abundance of the odd-n-alkanes was predominantly higher than the even-n-alkanes in the range of C_{25}-C_{33} (Fig. 6). Pristane and phytane appeared just in trace amount.

This study calculated several indices based on the n-alkane distribution: CPI (carbon preference index; Marzi et al. 1993); ACL (average chain length; Collister et al. 1994); Norm31 (proportional abundance of C_{29} and C_{31} n-alkanes); Norm33 (proportional abundance of C_{29} and C_{33} n-alkanes; Carr et al. 2014); and the proxy ratio Paq (relative proportion of mid-chain to long-chain n-alkanes, Ficken et al. 2000). These indices were shown in Table 7.

5 Discussion

5.1 Palaeoenvironmental conditions

There were no indications of morphological microfossils such as cyanobacterial filament traces or calcified sheaths in the study area, which are common in freshwater settings (Freytet and Verrecchia 1998, 1999; Arp et al. 2001). Likewise, well calcified cyanobacterial filaments or other algal fossils were not found in previous studies (Yi et al. 2008; Zeng et al. 2011). Furthermore,

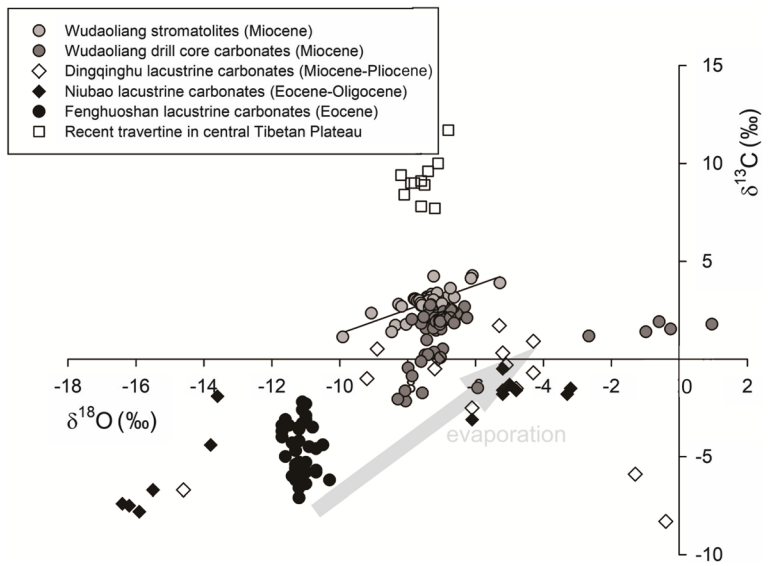

Fig. 4 Cross-plot for the stable carbon and oxygen isotope results of Wudaoliang stromatolites. Data of the Miocene Wudaoliang drill core carbonates are quoted from Wu et al. (2009); data of the Miocene-Pliocene Dingqinghu and the Eocene-Oligocene Niubao lacustrine carbonates are from Rowley and Currie (2006); data of the Eocene Fenghuoshan lacustrine carbonates are from Cyr et al. (2005); and, the data on the recent travertine in central Tibetan Plateau are from Niu et al. (2013). The greyish arrow indicates a trend of increasing evaporation from the Eocene to the Miocene in the northern Tibetan Plateau

no shelly fossils of eukaryotes (i.e., ostracods, gastropods, etc.) were observed in Wudaoliang stromatolites or other stromatolites of the Wudaoliang Group. However, in the argillaceous limestone and marlstone underlying and overlying the equivalent beds of Wudaoliang stromatolites, abundant ostracod (mostly *Eucypris*, few *Cyprinotus* and *Youshashanian*) and gastropod fossils (*Radix* sp. and *Gyraulus* sp.) were reported (Yi et al. 2000, 2008; Wu et al. 2008). *Eucypris* are a kind of common taxa in freshwater and brackish lake in northern Tibetan Plateau (Mischke et al. 2006; Wu et al. 2008); *Cyprinotus* is a taxon usually found from a saline lake (De Deckker 1981); and, *Youshashanian* usually appears in brackish to saline lake settings (Wu et al. 2008; Yang et al. 2006). *Radix* sp. and *Gyraulus* sp. are typical freshwater gastropods (Fontes et al. 1985; Taft et al. 2012). The total absence of all these fossils in the investigated stromatolites argues against a freshwater setting, and points to inhospitable ecological conditions during the stromatolite formation, such as high or strongly fluctuating salinity, high temperature, or toxic substances. Indeed, the only evidence of metazoa in the investigated stromatolites comes from elongated faecal pellets, which are similar to that of the brine shrimp *Artemia* pellets by similar size and shape (Fig. 3i; Eardley 1938; Kelts and Shahrabi 1986).

The presence of fenestral fabrics commonly reflects gas production and degradation in photosynthetic microbial mats, possibly indicating shallow sublittoral to littoral settings (Monty 1976; Hardie and Ginsburg 1977).

However, in the stromatolites investigated in this study, many of the fenestrae show angular outlines reminiscent of former evaporate crystals, while enclosed in vertically structured sublinear micrite resembling filamentous microbial mats (Fig. 3d-f). Besides, evaporate precipitation, specifically of gypsum, has been reported from a number of other stromatolites, reflecting high-salinity environments (Hudson 1970; Cater 1987; Arp et al. 2008; Allwood et al. 2013). Intercalated gypsum beds are also found between argillaceous marlstones of the Wudaoliang Group, indicating strong arid condition and intensive lake level fluctuations of the Miocene lake (Yi et al. 2000). In association with irregular fenestral fabrics, the possible calcite pseudomorphs after gypsum might present a frequently exposed supralittoral zone with high salinity. Although clear swallow-tail twin structures were not observed, the association of brine shrimp faecal pellets and co-varying stable carbon and oxygen isotopes (see below) are consistent with the interpretation of these angular traces as pseudomorphs after former evaporites.

5.2 Hydrology and evaporation

The covariation of $\delta^{13}C$ and $\delta^{18}O$ may be due to (1) hydrologically closed conditions of the lake basin and (2) mixed sampling between primary microcrystalline precipitates and diagenetic microspar, or both effects. However, there was no isotopic compositional difference between microspar-rich porous laminae and dense laminae. Thus, our data represented either complete diagenetic homogenization or primary signal during stromatolites formation. Zeng et al. (2011) measured the micritic calcites from laminae of

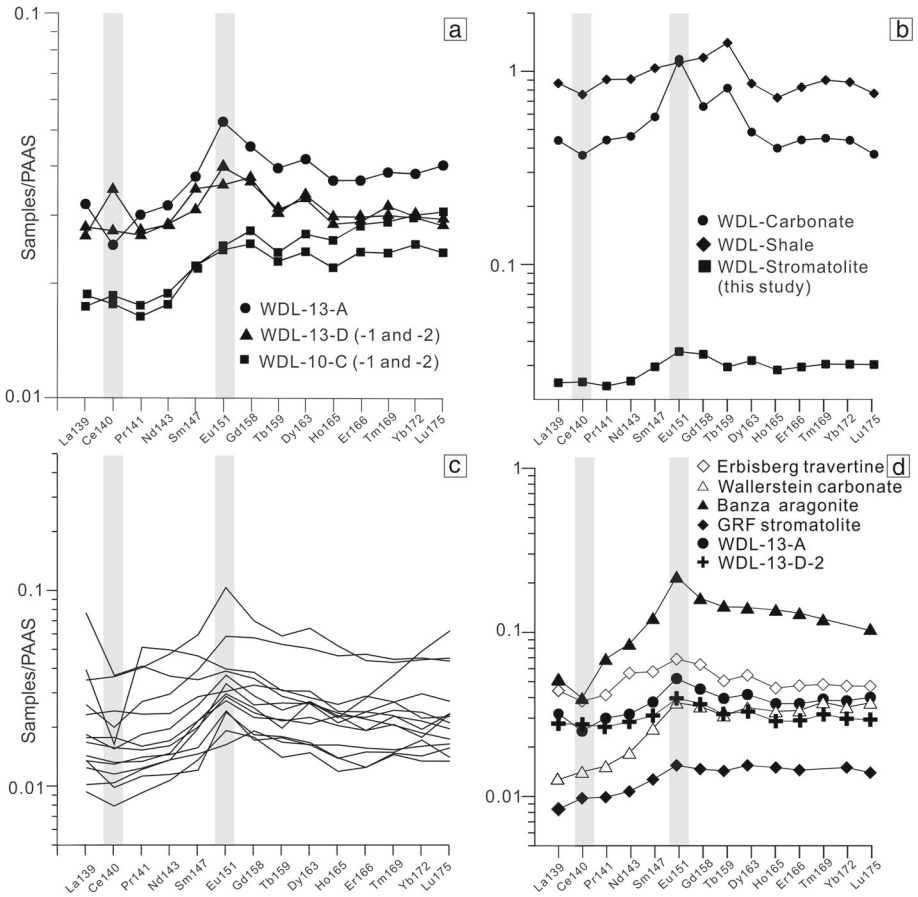

Fig. 5 PAAS-normalized rare earth element patterns of Wudaoliang stromatolites and reference samples. **a** PAAS-normalized REE patterns of samples WDL-13-A (ablation spot mode), WDL-13-D-1, WDL-13-D-2, WDL-10-C-1 and WDL-10-C-2 (line scan mode); **b** PAAS-normalized REE patterns of samples WDL-Carbonate, WDL-Shale, and WDL-Stromatolite. WDL-Carbonate and WDL-Shale were referred to the average REE composition of carbonate and shale of the Wudaoliang Group (Yi et al. 2008), WDL-Stromatolite was referred to the average REE composition of stromatolites in this study; **c** PAAS-normalized REE patterns of individually analysed laminae in sample WDL-13-A; **d** PAAS-normalized REE patterns of Wudaoliang stromatolites and reference samples. Banza aragonite (sample TGR21-I 1) was from Lake Tanganyika, East Africa (Barrat et al. 2000); Erbisberg travertine (Erb 1) and Wallerstein spring mound carbonate (Wa 98/8) were from Nördlinger Ries, western Bavaria, Germany (Arp et al. 2013); GRF stromatolite was from the Eocene Green River Formation, Wyoming, USA (Bolhar and Van Kranendonk 2007)

stromatolites in the Wudaoliang Group and obtained oxygen isotope data ranging from − 9.91‰ to − 5.28‰. Our isotopic results of calcite from different laminae were in accordance with Zeng et al. (2011) and thus showed pristine signals reflecting the hydrochemistry condition during the carbonate precipitation.

The $\delta^{18}O$ of Wudaoliang stromatolites in this study are similar to the carbonates in the Miocene Wudaoliang Group measured by Wu et al. (2009), despite a few argillaceous marlstone samples with higher $\delta^{18}O$ values (close to 0). During the Miocene Epoch, a vast lake system prevailed in Tibetan Plateau, marked by channels connected several lake sub-basins covering Hoh Xil and Lunpola areas (Wu et al. 2008; Polissar et al. 2009). Most of the sediments in the Wudaoliang Group are remarkable by a weak covariation of isotopic composition between $\delta^{18}O$ and $\delta^{13}C$ (Fig. 4), therefore representing a well-developed through-flowing, open lake episode during the Miocene vast lake system (Wu et al. 2008). Carbonates of the Eocene Fenghuoshan Formation in the Hoh Xil Basin showed a less variable oxygen isotope composition (− 11.7‰ to − 10.3‰) and retained a mean value around − 11‰, indicating a hydrologically open lake setting (Cyr et al. 2005). An Eocene-Pliocene evaporation trend in the Lunpola Basin was discussed (Rowley and Currie 2006; Polissar et al. 2009), meanwhile, a similar process took place in the Hoh Xil Basin, which confirmed that this climate changing trend was pronounced in the Tibetan Plateau.

The presence of Wudaoliang stromatolites indicates an aridification of the Miocene lake environment, representing a lake-level low-stand period. Evaporation preferentially removed ^{16}O from the water body, resulting in an ^{18}O enrichment in the residual water body. The lake level fall caused by evaporation finally resulted in

Table 3 Rare earth element (REE) concentrations (ppb) of Wudaoliang stromatolites and reference samples

Sample	La	Ce	Pr	Nd	Sm	Eu	Gd	Tb	Dy	Ho	Er	Tm	Yb	Lu	ΣREE	ΣLREE	ΣHREE
WDL-10-C-1	658	1480	155	600	124	27	128	18	117	26	82	11	84	13	3523	3044	479
WDL-10-C-2	705	1407	145	561	124	27	118	17	106	22	70	10	70	10	3392	2969	423
WDL-13-D-1	1006	2790	242	904	196	39	176	23	148	30	86	12	82	12	5746	5177	569
WDL-13-D-2	1058	2180	236	907	173	44	171	24	145	28	83	13	83	13	5158	4598	560
WDL-13-A	1214	2003	267	1015	211	58	212	30	184	37	107	15	107	17	5477	4768	709
WDL-Carbonate	16,670	29,400	3920	14,730	3250	1270	3090	630	2130	400	1280	180	1230	160	78,340	69,240	9100
WDL-Shale	32,950	60,590	8070	29,140	5810	1220	5530	1080	3800	730	2400	360	2460	330	154,470	137,780	16,690
Erbisberg travertine	1680	3050	368	1820	320	75	297	39	243	46	138	19	134	20	8249	7313	936
Wallerstein carbonate	481	1130	136	590	145	41	166	24	153	33	97	15	98	16	3125	2523	602
Banza aragonite	1962	3182	613	2722	684	240	759	110	626	137	379	–	306	45	11,765	9403	2362
GRF stromatolite	318	780	88	343	71	17	69	11	68	15	42	–	42	6	1870	1617	253

Note: WDL-13-A denoted the mean values of elemental concentration from 120 different point-ablation measurements in one stromatolite sample; WDL-Carbonate and WDL-Shale were referred to the averaging composition of carbonate and shale/mudstone in the Wudaoliang Group, data from Yi et al. (2008); Erbisberg hot-spring travertine (Erb 1) and Wallerstein spring mound carbonate (Wa 98/8) were from Arp et al. (2013); Banza sub-lacustrine hydrothermal-origin aragonite (TGR21-I 1) was from Barrat et al. (2000); GRF stromatolite meant the lacustrine freshwater stromatolite from Green River Formation studied by Bolhar and Van Kranendonk (2007)

hypersaline conditions and temporary subaerial exposure, in accordance with the presence of fenestral fabrics, absence of eukaryotic fossils and possible gypsum pseudomorphs. Thus, for the formation of the investigated Wudaoliang stromatolites, a hypersaline lacustrine environment due to evaporation is more convincing than a freshwater setting.

Wudaoliang stromatolites show $\delta^{13}C$ values ranging from 2.43‰ to 4.12‰, about 1.20‰ higher than skeletal limestones (Yi et al. 2008) and marlstones (Wu et al. 2009) of the same formation. High $\delta^{13}C$ values might point to a significant photosynthetic effect in the water body. In photosynthetic process ^{12}C is preferentially assimilated by primary producers, resulting $^{13}C_{DIC}$ enrichment in lake water and high $\delta^{13}C$ in the carbonates (Kerby and Raven 1985; Hollander and McKenzie 1991; Gu et al. 1996). Therefore, despite high salinity, a significant primary carbon production is evident for this depositional period of the lake in the Hoh Xil Basin.

5.3 Possible hydrothermal impact on stromatolites

The ΣREE values of Wudaoliang stromatolites were much lower than the skeletal carbonates from the Wudaoliang Group (Fig. 5b, Yi et al. 2008). Samples WDL-10-C-1, WDL-10-C-2 and WDL-13-A showed slightly enrichment of HREEs. But no significant enrichment of LREEs or HREEs was shown for Wudaoliang stromatolites, as low La/Lu_{SN} ratios were close to 1, arguing against highly-alkaline, soda lake conditions (e.g., Mono lake in USA, Johannesson and Lyons 1994). Further, higher ΣREE were detected in the dense laminae

Table 4 PAAS-normalized REE values of Wudaoliang stromatolites and their reference samples

Sample	La_{SN}	Ce_{SN}	Pr_{SN}	Nd_{SN}	Sm_{SN}	Eu_{SN}	Gd_{SN}	Tb_{SN}	Dy_{SN}	Ho_{SN}	Er_{SN}	Tm_{SN}	Yb_{SN}	Lu_{SN}	La/Lu_{SN}	Ce/Ce^*_{SN}	Eu/Eu^*_{SN}
WDL-10-C-1	0.017	0.019	0.017	0.019	0.022	0.025	0.027	0.024	0.027	0.026	0.028	0.029	0.030	0.030	0.568	1.070	1.006
WDL-10-C-2	0.019	0.018	0.016	0.018	0.022	0.024	0.025	0.023	0.024	0.022	0.024	0.024	0.025	0.024	0.778	1.010	1.028
WDL-13-D-1	0.026	0.035	0.027	0.028	0.035	0.036	0.037	0.030	0.034	0.030	0.030	0.030	0.029	0.028	0.944	1.300	0.989
WDL-13-D-2	0.028	0.027	0.027	0.028	0.031	0.040	0.036	0.031	0.033	0.028	0.029	0.032	0.030	0.029	0.955	1.000	1.184
WDL-13-A	0.032	0.025	0.030	0.032	0.038	0.052	0.045	0.040	0.042	0.037	0.037	0.039	0.038	0.040	0.794	0.810	1.260
WDL-Carbonate	0.439	0.368	0.440	0.460	0.580	1.155	0.657	0.818	0.484	0.400	0.441	0.450	0.439	0.372	1.179	0.840	1.770
WDL-Shale	0.867	0.757	0.907	0.911	1.038	1.109	1.177	1.403	0.864	0.730	0.828	0.900	0.879	0.767	1.130	0.850	0.950
Erbisberg travertine	0.044	0.038	0.041	0.057	0.057	0.068	0.063	0.051	0.055	0.046	0.048	0.048	0.048	0.047	0.951	0.891	1.133
Wallerstein carbonate	0.013	0.014	0.015	0.018	0.026	0.037	0.035	0.031	0.035	0.033	0.033	0.038	0.035	0.037	0.340	1.011	1.218
Banza aragonite	0.052	0.040	0.069	0.085	0.122	0.218	0.161	0.143	0.142	0.137	0.131	–	0.109	0.105	0.492	0.660	1.538
GRF stromatolite	0.008	0.010	0.010	0.011	0.013	0.015	0.015	0.014	0.015	0.015	0.014	–	0.015	0.014	0.600	1.068	1.130

Table 5 Integration of rare earth element (REE) concentrations in stromatolite laminae of the sample WDL-13-A

Laminae type	La	Ce	Pr	Nd	Sm	Eu	Gd	Tb	Dy	Ho	Er	Tm	Yb	Lu	ΣREE	ΣLREE	ΣHREE
Dense (*n* = 8)	1679	3695	456	1931	422	145	416	57	358	66	161	22	157	25	9590	8328	1240
Dense (n = 8)	1120	2464	263	956	204	43	196	30	158	33	106	14	105	15	5707	5050	643
Porous (n = 8)	854	1803	181	695	154	38	134	21	116	29	71	10	63	13	4182	3725	447
Dense (n = 8)	1909	1664	580	2016	329	55	228	30	171	31	88	12	69	13	7195	6553	630
Porous (*n* = 7)	744	1506	182	673	128	39	117	20	103	24	66	9	65	10	3686	3272	405
Dense (n = 8)	3707	3753	464	1481	249	54	212	28	148	27	88	14	79	12	10,316	9708	594
Porous (n = 8)	808	1605	173	654	142	40	141	21	125	26	71	12	76	11	3905	3422	471
Dense (*n* = 6)	920	1792	201	798	204	55	200	26	200	38	139	25	232	45	4875	3970	880
Porous (n = 6)	655	1407	184	737	187	62	206	35	197	40	108	14	89	13	3934	3232	688
Dense (*n* = 5)	959	1874	224	886	166	36	183	26	145	28	88	12	98	12	4737	4145	580
Porous (n = 5)	724	1284	167	696	155	43	170	22	132	24	74	12	76	12	3591	3069	510
Dense (n = 6)	1182	2101	277	1065	246	69	230	32	202	39	110	17	113	15	5698	4940	741
Porous (n = 6)	870	1331	170	622	115	44	146	23	124	24	61	10	68	11	3619	3152	457
Dense (n = 8)	1259	2021	306	1201	280	82	342	52	282	59	174	23	161	24	6266	5149	1094
Porous (n = 5)	736	1440	165	694	137	37	166	23	111	22	78	10	66	11	3696	3209	477
Dense (n = 8)	914	1780	224	989	248	70	287	43	354	78	225	36	214	39	5501	4225	1240
Porous (*n* = 10)	859	1675	180	698	140	44	170	20	137	25	76	10	80	12	4126	3596	520
Mean dense laminae	1496	2181	317	1174	241	58	235	33	207	42	127	19	134	22	6286	5467	800
Mean porous laminae	881	1749	206	822	175	55	185	27	156	31	85	12	82	13	4479	3888	579

than in the porous laminae, as is the case with the sample WDL-13-A (Table 3).

Although low in Eu concentration, the Eu anomaly of Wudaoliang stromatolites was significant, as shown by its consistent presence in most of the analysed laminae (Fig. 5c). Sample WDL-13-A showed the most prominent positive Eu anomaly. Indeed, the Eu anomalies did not correlate with aluminium ($r = 0.11$, $p = 0.664$) or silica ($r = 0.06$, $p = 0.819$) contents. These Eu anomalies were thus not affected by terrestrial inputs or decomposition of Eu-enriched minerals

Table 6 Integration of PAAS-normalized REE values in stromatolite laminae of the sample WDL-13-A

Laminae type	La_{SN}	Ce_{SN}	Pr_{SN}	Nd_{SN}	Sm_{SN}	Eu_{SN}	Gd_{SN}	Tb_{SN}	Dy_{SN}	Ho_{SN}	Er_{SN}	Tm_{SN}	Yb_{SN}	Lu_{SN}	La/Lu_{SN}	Ce/Ce^*_{SN}	Eu/Eu^*_{SN}
Dense (n = 8)	0.044	0.046	0.051	0.060	0.075	0.132	0.089	0.074	0.081	0.066	0.056	0.054	0.056	0.057	0.771	0.968	1.608
Dense (n = 8)	0.029	0.031	0.030	0.030	0.036	0.039	0.042	0.039	0.036	0.033	0.037	0.034	0.038	0.034	0.856	1.043	0.993
Porous (n = 8)	0.022	0.023	0.020	0.022	0.027	0.035	0.028	0.028	0.026	0.029	0.024	0.026	0.023	0.030	0.756	1.054	1.242
Dense (n = 8)	0.050	0.021	0.065	0.063	0.059	0.050	0.048	0.039	0.039	0.031	0.030	0.029	0.025	0.030	1.683	0.360	0.940
Porous (n = 7)	0.020	0.019	0.020	0.021	0.023	0.035	0.025	0.026	0.024	0.024	0.023	0.022	0.023	0.024	0.821	0.942	1.476
Dense (n = 8)	0.098	0.047	0.052	0.046	0.044	0.049	0.045	0.037	0.034	0.027	0.030	0.034	0.028	0.029	3.376	0.627	1.103
Porous (n = 8)	0.021	0.020	0.019	0.020	0.025	0.037	0.030	0.027	0.028	0.026	0.024	0.029	0.027	0.025	0.854	0.986	1.319
Dense (n = 6)	0.024	0.022	0.023	0.025	0.036	0.050	0.043	0.033	0.045	0.038	0.048	0.062	0.083	0.105	0.230	0.956	1.273
Porous (n = 6)	0.017	0.018	0.021	0.023	0.033	0.057	0.044	0.045	0.045	0.040	0.037	0.035	0.032	0.029	0.586	0.929	1.468
Dense (n = 5)	0.025	0.023	0.025	0.028	0.030	0.033	0.039	0.034	0.033	0.028	0.030	0.030	0.035	0.028	0.888	0.930	0.965
Porous (n = 5)	0.019	0.016	0.019	0.022	0.028	0.039	0.036	0.028	0.030	0.024	0.025	0.029	0.027	0.027	0.699	0.848	1.227
Dense (n = 6)	0.031	0.026	0.031	0.033	0.044	0.063	0.049	0.041	0.046	0.039	0.038	0.041	0.040	0.036	0.872	0.844	1.351
Porous (n = 6)	0.023	0.017	0.019	0.019	0.020	0.040	0.031	0.030	0.028	0.024	0.021	0.025	0.024	0.027	0.862	0.793	1.568
Dense (n = 8)	0.033	0.025	0.034	0.038	0.050	0.074	0.073	0.067	0.064	0.059	0.060	0.056	0.057	0.055	0.599	0.749	1.212
Porous (n = 5)	0.019	0.018	0.019	0.022	0.025	0.033	0.035	0.030	0.025	0.022	0.027	0.025	0.023	0.025	0.776	0.948	1.111
Dense (n = 8)	0.024	0.022	0.025	0.031	0.044	0.064	0.061	0.056	0.081	0.078	0.078	0.089	0.076	0.090	0.268	0.904	1.213
Porous (n = 10)	0.023	0.021	0.020	0.022	0.025	0.040	0.036	0.026	0.031	0.025	0.026	0.025	0.029	0.027	0.830	0.979	1.319

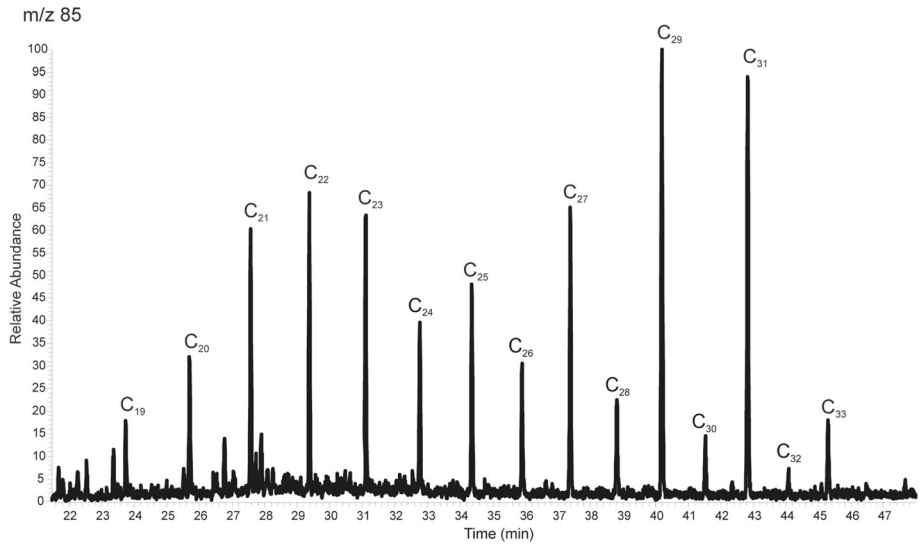

Fig. 6 Bimodal distribution pattern of the relative abundance of normal alkane detected in the stromatolite samples ranging from the mid-chain n-alkanes (C_{19} to C_{24}) to the long-chain n-alkanes (C_{25} to C_{35}). Note the predominance of odd-numbered n-alkanes over even-numbered n-alkanes in their relative abundance range in the range of C_{25}-C_{33}. Long-chain odd-numbered n-alkanes (C_{25}, C_{27}, C_{29}, C_{31}) could indicate the presence of higher plants in the vicinity of the depositional environment. See further explanation from the calculated index results in Table 7

(e.g., plagioclase, Sverjensky 1984; Bau 1991). Eu enrichment has been used to identify hydrothermal activities, because its mobility and redox state are closely related to the high temperature (Michard 1989; Mills and Elderfield 1995; Barrat et al. 2000).

For a better comparison, we plotted REE patterns for the aragonites precipitated from mixed sub-lacustrine hydrothermal fluid and lake water (Banza aragonite, Barrat et al. 2000), the carbonates affected by deep hydrothermal or hot spring activities (Erbisberg hot spring travertine and Wallerstein spring mound carbonate, Arp et al. 2013), and the stromatolites deposited in a freshwater lake (Green River Formation, Bolhar and Van Kranendonk 2007) on Fig. 5d. The REE patterns of Wudaoliang stromatolites are similar to the patterns of the reference samples as Banza aragonite, Erbisberg travertine and Wallerstein carbonate. In addition, stromatolites at other locations of the Wudaoliang Group formed only centimeter- to decimeter-thick beds, while the localized extensive thick-bedded occurrence of stromatolites at the slope section north of Wudaoliang Town, i.e. the Wudaoliang stromatolites in this study, possibly suggested a localized hydrothermal spring influx at this area. The hydrothermal origin of the fluids is evident from the positive Eu anomaly of the stromatolites. Nonetheless, a prominent mound structure was not evident in the sample site, so that the past hydrothermal fluids might have been introduced by the diffused sub-lacustrine spring or the surface hot spring runoff.

Furthermore, we compared the oxygen isotope of Wudaoliang stromatolites with the Holocene travertines in the Qiangtang Basin (Niu et al. 2013). The source water of the hot spring travertines is of meteoric origin (Tian et al. 2001; Zhang et al. 2002). A significantly elevated $\delta^{13}C$ (up to 11.7‰) is found in these travertines, possibly related to a deep source of CO_2 (Tian et al. 2001; Zhang et al. 2002). Similar $\delta^{18}O$ values of stromatolites to those of the Holocene travertines thus may also indicate a mixed origin of hydrothermal fluids with the Miocene period local rainfall, presuming the monsoon precipitation was similar to present conditions. However, uncertainty remains with this hypothesis, since the monsoon precipitation on northern Tibetan Plateau could have had different isotopic composition during the

Table 7 Calculated index results based on biomarker parameters of the analyzed stromatolites

Index	Calculation	Result
CPI_{25-31}	$0.5 \times [(n\text{-}C_{25} + n\text{-}C_{27} + n\text{-}C_{29} + n\text{-}C_{31})/(n\text{-}C_{24} + n\text{-}C_{26} + n\text{-}C_{28} + n\text{-}C_{30}) + (n\text{-}C_{25} + n\text{-}C_{27} + n\text{-}C_{29} + n\text{-}C_{31})/(n\text{-}C_{26} + n\text{-}C_{28} + n\text{-}C_{30} + n\text{-}C_{32})]$	3.79
ACL_{27-33}	$(27 \times n\text{-}C_{27} + 29 \times n\text{-}C_{29} + 31 \times n\text{-}C_{31} + 33 \times n\text{-}C_{33})/(n\text{-}C_{27} + n\text{-}C_{29} + n\text{-}C_{31} + n\text{-}C_{33})$	29.53
Norm31	$n\text{-}C_{31}/(n\text{-}C_{29} + n\text{-}C_{31})$	0.49
Norm33	$n\text{-}C_{33}/(n\text{-}C_{29} + n\text{-}C_{33})$	0.15
Paq	$(C_{23} + C_{25})/(C_{23} + C_{25} + C_{29} + C_{31})$	0.34

Miocene (see Polissar et al. 2009). Further studies are required to address this problem.

5.4 Surrounding ecology

C_{org} content in Wudaoliang stromatolites was less than 0.1 wt%; and the poor biomarker preservation was also consistent with the C_{org} content: there was no indication of specific microbial groups involving in the stromatolite formation.

Long-chain odd-numbered n-alkanes (C_{25}, C_{27}, C_{29}, C_{31}) indicate the presence of higher plants in the vicinity of the stromatolite-forming lake. In general, n-alkanes produced by forests may have a prominent n-C_{29} > n-C_{31} pattern, whereas grassland background may show a n-C_{31} > n-C_{29} pattern (Kuhn et al. 2010; Rao et al. 2011). ACL values around 29.53 can be characteristic for different kinds of trees (Hoffmann et al. 2013). The Paq ratio of 0.34 can indicate for a mixture of shallow surface sediments with some green algae from the Qinghai Lake, northern Tibetan Plateau (Liu et al. 2015). A Norm31 value of 0.49 is similar to values calculated from leaf samples of different species of Compositae (Guo et al. 2016) in differing altitudes, and also from montane plants and soils (Carr et al. 2014). However, these patterns may vary with respect to local vegetation, altitude and humid or dry climate (Rao et al. 2011; Zhang et al. 2017), therefore, revealing more detailed palaeoenvironment information is not clearly possible.

6 Conclusions

In summary, this study interpreted a hypersaline setting for Wudaoliang stromatolites. Spar-cemented, angular fenestrae enclosed in a vertically structured micrite framework were explained as evaporite pseudomorphs within calcifying microbial mats. The association of brine-shrimp faecal pellets, absence of other eukaryotic fossils, and covariation of stable isotopes further supported the interpretation of a frequently exposed and evaporated, hypersaline littoral setting.

The oxygen isotope data of stromatolite calcites were in accordance with previously published results, and the coordinated variation of $\delta^{13}C$ and $\delta^{18}O$ indicates a hydrologically closed lake setting. A higher $\delta^{13}C$ in comparison to the Miocene skeletal carbonates suggested a significant photosynthetic activity in the lake during the growth of Wudaoliang stromatolites.

The possibility of hydrothermal inflow to the Miocene lake was supported by a positive Eu anomaly in the stromatolites. A hydrothermal inflow could also explain the localized occurrence of the up-to-15-m-thick stromatolitic deposits. There is no indication of a freshwater setting at the time of stromatolite formation.

Abbreviations

ACL: Average chain length; CNS: Carbon-nitrogen-sulfur (analysis); CPI: Carbon preference index; Norm31: Proportional abundance of C_{29} and C_{31} n-alkanes; Norm33: Proportional abundance of C_{29} and C_{33} n-alkanes; Paq: Relative proportion of mid-chain to long-chain n-alkanes; SBS: Stromatolite bearing section

Acknowledgements

The authors would like to acknowledge Prof. Ming-Cai Hou, the head of the Institute of Sedimentary Geology in Chengdu University of Technology, for his supporting; and Prof. Zhi-Qiang Shi for his kindly help on the stable oxygen and carbon isotope measurements. Also, many thanks to Mr. Axel Hackmann for his assistance on thin sections; to Dr. Andreas Reimer and Mrs. Birgit Röring for their kind help with the carbon-nitrogen-sulfur content measurement; to Dr. Shi-Tou Wu for his assistance in LA-ICP-MS. Many thanks to Prof. Zeng-Zhao Feng, Prof. Stephen Kershaw, two anonymous reviewers and editors of the *JoP* for their constructive suggestions and corrections, which significantly improved the manuscript.

Funding

This study is funded by the National Natural Science Foundation of China (Grant Nos. 41772105 and 41402099).

Availability of data and materials

Information of data and material(s) was in figures and tables of the manuscript.

Authors' contributions

LQZ carried out the thin-section investigation, the carbon and oxygen isotope data and REE data analysis and interpretation, and composed the manuscript; HSY organized the field work and offered samples; GQX joined the field work; KS carried out the LA-ICP-MS analysis; CH carried out the biomarker analysis; GA helped draft the manuscript. All authors read and approved the final manuscript.

Competing interests

The authors declare that they have no competing interests.

Publisher's Note

Author details

[1]Institute of Sedimentary Geology, Chengdu University of Technology, Chengdu 610059, Sichuan Province, China. [2]State Key Laboratory of Oil and Gas Reservoir Geology and Exploitation, Chengdu 610059, Sichuan Province, China. [3]Geoscience Center, Georg-August-Universität Göttingen, Goldschmidtstraße 3, 37077 Göttingen, Germany.

Received: 14 March 2019 Accepted: 31 March 2019
Published online: 02 May 2019

References

Allwood, A., I. Burch, J. Rouchy, and M. Coleman. 2013. Morphological biosignatures in gypsum: Diverse formation processes of Messinian (~6.0 ma) gypsum stromatolites. *Astrobiology* 13 (9): 870–886.

Arp, G., C. Kolepka, K. Simon, V. Karius, N. Nolte, and B.T. Hansen. 2013. New evidence for persistent impact-generated hydrothermal activity in the Miocene Ries impact structure, Germany. *Meteorite and Planetary Science* 48 (12): 2491–2516.

Arp, G., C. Ostertag-Henning, S. Yuecekent, J. Reitner, and V. Thiel. 2008. Methane-related microbial gypsum calcitization in stromatolites of a marine evaporative setting (Münder formation, upper Jurassic, Hils syncline, North Germany). *Sedimentology* 55 (5): 1227–1251.

Arp, G., A. Reimer, and J. Reitner. 2001. Photosynthesis-induced biofilm calcification and calcium concentrations in Phanerozoic oceans. *Science* 292 (5522): 1701–1704.

Barrat, J., J. Boulegue, J. Tiercelin, and M. Lesourd. 2000. Strontium isotopes and rare-earth element geochemistry of hydrothermal carbonate deposits from Lake Tanganyika, East Africa. *Geochimica et Cosmochimica Acta* 64 (2): 287–298.

Bau, M. 1991. Rare-earth element mobility during hydrothermal and metamorphic fluid-rock interaction and the significance of the oxidation state of europium. *Chemical Geology* 93 (3–4): 219–230.

Bolhar, R., and M.J. Van Kranendonk. 2007. A non-marine depositional setting for the northern Fortescue group, Pilbara craton, inferred from trace element geochemistry of stromatolitic carbonates. *Precambrian Research* 155 (3–4): 229–250.

Carr, A.S., A. Boom, H.L. Grimes, B.M. Chase, M.E. Meadows, and A. Harris. 2014. Leaf wax n-alkane distributions in arid zone south African flora: Environmental controls, chemotaxonomy and palaeoecological implications. *Organic Geochemistry* 67: 72–84.

Cater, J.M. 1987. Sedimentology of part of the lower oil-shale group (Dinantian) sequence at Granton, Edinburgh, including the Granton "shrimp-bed". *Earth and Environmental Science Transactions of the Royal Society of Edinburgh* 78 (1): 29–40.

Collister, J.W., G. Rieley, B. Stern, G. Eglinton, and B. Fry. 1994. Compound-specific $\delta^{13}C$ analyses of leaf lipids from plants with differing carbon dioxide metabolisms. *Organic Geochemistry* 21: 619–627.

Cyr, A.J., B.S. Currie, and D.B. Rowley. 2005. Geochemical evaluation of Fenghuoshan group lacustrine carbonates, north-Central Tibet: Implications for the paleoaltimetry of the Eocene Tibetan plateau. *The Journal of Geology* 5: 517–533.

De Deckker, P. 1981. Ostracods of a thalassic saline lakes. In *Salt Lakes. Developments in Hydrobiology*, ed. W.D. Williams, vol. 5, 131–144. Dordrecht: Springer.

Demicco, R.V., and L.A. Hardie. 1994. *Sedimentary structures and early diagenetic features of shallow marine carbonate deposits. SEPM Atlas Series No. 1. SEPM Society for Sedimentary*.

Eardley, A.J. 1938. Sediments of great salt Lake, Utah. *AAPG Bulletin* 22: 1305–1411.

Ficken, K.J., B. Li, D. Swain, and G. Eglinton. 2000. An n-alkane proxy for the sedimentary input of submerged/floating freshwater aquatic macrophytes. *Organic Geochemistry* 31 (7–8): 745–749.

Fontes, J.C., F. Gasse, Y. Callot, J.C. Plaziat, P. Carbonel, P. Dupeuble, and I. Kaczmarska. 1985. Freshwater to marine-like environments from Holocene lakes in northern Sahara. *Nature* 317 (6038): 608.

Freytet, P., and E. Verrecchia. 1998. Freshwater organisms that build stromatolites: A synopsis of biocrystallization by prokaryotic and eukaryotic algae. *Sedimentology* 45 (3): 535–563.

Freytet, P., and E. Verrecchia. 1999. Calcitic radial palisadic fabric in freshwater stromatolites: Diagenetic and recrystallized feature or physicochemical sinter crust? *Sedimentary Geology* 126 (1–4): 97–102.

Gu, B., C. Schelske, and M. Hoyer. 1996. Stable isotopes of carbon and nitrogen as indicators of diet and trophic structure of the fish community in a shallow hypereutrophic lake. *Journal of Fish Biology* 49 (6): 1233–1243.

Guo, N., J. Gao, Y. He, and Y. Guo. 2016. Compositae plants differed in leaf cuticular waxes between high and low altitudes. *Chemistry and Biodiversity* 13 (6): 710–718.

Hao, H., Y. Song, L. Li, Z. Jia, Y. Wang, and Q. Liu. 2015. Characteristics of breccias and C-O-Sr-S isotope geochemistry of the Duocaima Pb-Zn deposit in Tuotuohe, Qinghai Province: Implications for the ore-forming process. *Acta Geologica Sinica (English Edition)* 89 (5): 1568–1587.

Hardie, L.A., and R.N. Ginsburg. 1977. Layering: The origin and environmental significance of lamination and thin bedding. In *Sedimentation on the Modern Carbonate Tidal Flats of Northwest Andros Island, Bahamas. Baltimore, Studies in Geology*, ed. L.A. Hardie, vol. 22, 12–49. Maryland: The Johns Hopkins University Press.

Hoffmann, B., A. Kahmen, L.A. Cernusak, S.K. Arndt, and D. Sachse. 2013. Abundance and distribution of leaf wax n-alkanes in leaves of Acacia and Eucalyptus trees along a strong humidity gradient in northern Australia. *Organic Geochemistry* 62: 62–67.

Hollander, D.J., and J.A. McKenzie. 1991. CO_2 control on carbon-isotope fractionation during aqueous photosynthesis: A paleo-pCO_2 barometer. *Geology* 19 (9): 929–932.

Hudson, J.D. 1970. Algal limestones with pseudomorphs after gypsum from the middle Jurassic of Scotland. *Lethaia* 3 (1): 11–40.

Johannesson, K.H., and W.B. Lyons. 1994. The rare earth element geochemistry of mono Lake water and the importance of carbonate complexing. *Limnology Oceanography* 39 (5): 1141–1154.

Kelts, K., and M. Shahrabi. 1986. Holocene sedimentology of hypersaline Lake Urmia, northwestern Iran. *Palaeogeography, Palaeoclimatology, Palaeoecology* 54 (1): 105–130.

Kerby, N., and J.A. Raven. 1985. Transport and fixation of inorganic carbon by marine algae. *Advances in Botanical Research* 11: 71–123.

Kuhn, T.K., E.S. Krull, A. Bowater, K. Grice, and G. Gleixner. 2010. The occurrence of short chain n-alkanes with an even over odd predominance in higher plants and soils. *Organic Geochemistry* 41 (2): 88–95.

Liu, W., H. Yang, H. Wang, Z. An, Z. Wang, and Q. Leng. 2015. Carbon isotope composition of long chain leaf wax n-alkanes in lake sediments: A dual indicator of paleoenvironment in the Qinghai-Tibet plateau. *Organic Geochemistry* 83: 190–201.

Marzi, R., B. Torkelson, and R. Olson. 1993. A revised carbon preference index. *Organic Geochemistry* 20 (8): 1303–1306.

Michard, A. 1989. Rare earth element systematics in hydrothermal fluids. *Geochimica et Cosmochimica Acta* 53 (3): 745–750.

Mills, R.A., and H. Elderfield. 1995. Rare earth element geochemistry of hydrothermal deposits from the active TAG mound, 26 N mid-Atlantic ridge. *Geochimica et Cosmochimica Acta* 59 (17): 3511–3524.

Mischke, S., U. Herzschuh, Z. Sun, Z. Qiao, N. Sun, and A.M. Zander. 2006. Middle Pleistocene Ostracoda from a large freshwater lake in the presently dry Qaidam Basin (NW China). *Journal of Micropalaeontology* 25: 57–64.

Monty, C. 1976. The origin and development of Cryptalgal fabrics. In *Developments in Sedimentology*, ed. M.R. Walter, 193–249. Amsterdam: Elsevier.

Niu, X., X. Liu, and W. Chen. 2013. Travertine in south Bank of Dogai Coring, Tibet: Geochemical characteristics and potash geological significance. *Acta Sedimentologica Sinica* 31: 1031–1040 (in Chinese with English abstract).

Polissar, P.J., K.H. Freeman, D.B. Rowley, F.A. McInerney, and B.S. Currie. 2009. Paleoaltimetry of the Tibetan plateau from D/H ratios of lipid biomarkers. *Earth and Planetary Science Letter* 287 (1–2): 64–76.

Rao, Z., Y. Wu, Z. Zhu, G. Jia, and A. Henderson. 2011. Is the maximum carbon number of long-chain n-alkanes an indicator of grassland or forest? Evidence from surface soils and modern plants. *Chinese Science Bulletin* 56 (16): 1714–1720.

Riding, R. 1991. Calcified cyanobacteria. In *Calcareous algae and stromatolites*, ed. R. Riding, 55–87. Berlin, Heidelberg: Springer.

Riding, R. 2000. Microbial carbonates: The geological record of calcified bacterial–algal mats and biofilms. *Sedimentology* 47: 179–214.

Rowley, D.B., and B.S. Currie. 2006. Palaeo-altimetry of the late Eocene to Miocene Lunpola Basin, Central Tibet. *Nature* 7077: 677.

Surdam, R.C., and J.L. Wray. 1976. Lacustrine Stromatolites, Eocene Green River Formation, Wyoming. In *Developments in Sedimentology*, ed. M.R. Walter, 535–541. Armsterdam: Elsevier.

Sverjensky, D.A. 1984. Europium redox equilibria in aqueous solution. *Earth and Planetary Science Letter* 67 (1): 70–78.

Taft, L., U. Wiechert, F. Riedel, M. Weynell, and H. Zhang. 2012. Sub-seasonal oxygen and carbon isotope variations in shells of modern *Radix* sp. (Gastropoda) from the Tibetan plateau: Potential of a new archive for palaeoclimatic studies. *Quaternary Science Reviews* 34: 44–56.

Tian, L., V. Masson-Delmotte, M. Stievenard, T. Yao, and J. Jouzel. 2001. Tibetan plateau summer monsoon northward extent revealed by measurements of water stable isotopes. *Journal of Geophysical Research: Atmospheres* 106 (D22): 28081–28088.

Wang, C., Z. Liu, H. Yi, S. Liu, and X. Zhao. 2002. Tertiary crustal shortening and peneplanation in the Hoh Xil region: Implications for the tectonic history of the northern Tibetan plateau. *Journal of Asian Earth Science* 20 (3): 211–223.

Wang, C., X. Zhao, Z. Liu, P.C. Lippert, S.A. Graham, R.S. Coe, H. Yi, L. Zhu, S. Liu, and Y. Li. 2008. Constraints on the early uplift history of the Tibetan plateau. *Proceedings of the National Academy of Sciences* 105 (13): 4987–4992.

Wu, Z., P.J. Barosh, Z. Wu, D. Hu, X. Zhao, and P. Ye. 2008. Vast Early Miocene lakes of the central Tibetan plateau Miocene lakes of Tibet. *Geological Society of America Bulletin* 120 (9–10): 1326–1337.

Wu, Z., Z. Wu, D. Hu, and H. Peng. 2009. Carbon and oxygen isotope changes and palaeoclimate cycles recorded by lacustrine deposits of Miocene Wudaoliang group in northern Tibetan plateau. *Geology in China* 36 (5): 966–975 (in Chinese with English abstract).

Yang, F., Z.Z. Qiao, H.Q. Zhang, Y. Zhang, and Z.C. Sun. 2006. Features of the Cenozoic ostracod fauna and environmental significance in Qaidam Basin. *Journal of Palaeogeography (Chinese Edition)* 8 (2): 143–156 (in Chinese with English abstract).

Yi, H., C. Wang, S. Liu, Z. Liu, and S. Wang. 2000. Sedimentary record of the planation surface in the Hoh Xil region of the northern Tibet plateau. *Acta Geologica Sinica (English Edition)* 74 (4): 827–835.

Yi, H.S., J.H. Lin, K.K. Zhou, J.P. Li, and H.G. Huang. 2008. The origin of Miocene lacustrine stromatolites in the Hoh Xil area and its palaeoclimatic

implications. *Journal of Mineralogy and Petrology* 28 (1): 106–113 (in Chinese with English abstract).

Zeng, D.Y., Z.Q. Shi, H. Zhang, Y.Y. Wang, H.L. Liu, and J.F. Tian. 2011. Characters and classification of Miocene lacustrine stromatolites in Wudaoliang area, northern Tibetan plateau: Implications for paleoclimate. *Journal of Mineralogy and Petrology* 31 (3): 111–119 (in Chinese with English abstract).

Zhang, X., M. Nakawo, T. Yao, J. Han, and Z. Xie. 2002. Variations of stable isotopic compositions in precipitation on the Tibetan plateau and its adjacent regions. *Science in China Earth Sciences* 45 (6): 481–493.

Zhang, X., B. Xu, F. Günther, I. Mügler, M. Lange, H. Zhao, J. Li, and G. Gleixner. 2017. Hydrogen isotope ratios of terrestrial leaf wax n-alkanes from the Tibetan plateau: Controls on apparent enrichment factors, effect of vapor sources and implication for altimetry. *Geochimica et Cosmochimica Acta* 211: 10–27.

Zhang, X.F., M.P. Zheng, W.X. Chen, C.Y. Ye, Y.B. Luo, and W.G. Kong. 2015. Some new opinions concerning the genesis of the lacustrine hydrothermal deposits in Wudaoliang formation, eastern Hoh Xil Basin. *Acta Geoscientica Sinica* 36 (4): 507–512 (in Chinese with English Abstract).